Novel workflow for combining Raman spectroscopy and MALDI-MSI for tissue based studies

Thomas Bocklitz[1] · Katharina Bräutigam[1] · Annett Urbanek[2] ·
Franziska Hoffmann[3] · Ferdinand von Eggeling[1,3,4,5] · Günther Ernst[3] ·
Michael Schmitt[1] · Ulrich Schubert[2,4] · Orlando Guntinas-Lichius[3] · Jürgen Popp[1,5]

Abstract Molecular heterogeneity of cancer is a major obstacle in tumor diagnosis and treatment. To deal with this heterogeneity, a multidisciplinary combination of different analysis techniques is of urgent need because a combination enables the creation of a multimodal image of a tumor. Here, we develop a computational workflow in order to combine matrix-assisted laser desorption/ionization mass spectrometric (MALDI-MS) imaging and Raman microspectroscopic imaging for tissue based studies. The computational workflow can be used to confirm a spectral histopathology (SHP) based on one technique with another technique. In this contribution, we confirmed a Raman spectroscopic based SHP with MALDI-imaging. Owing to this combination, we could demonstrate, for a larynx carcinoma sample, that tissue types and different metabolic states could be extracted from the Raman spectra. Further investigations with the help of MALDI spectra yield a better characterization of variable epithelial differentiation and a better understanding of ongoing dysplastic alterations.

Keywords Raman spectroscopic imaging · MALDI-MS imaging · Multimodal imaging · Cancer

Thomas Bocklitz and Katharina Bräutigam contributed equally to this work and share main authorship.

✉ Thomas Bocklitz
thomas.bocklitz@uni-jena.de

✉ Jürgen Popp
juergen.popp@ipht-jena.de

[1] Institute of Physical Chemistry and Abbe Center of Photonics, University of Jena, Helmholtzweg 4, 07743 Jena, Germany

[2] Laboratory of Organic and Macromolecular Chemistry (IOMC), Friedrich Schiller University Jena, Humboldtstraße 10, 07743 Jena, Germany

[3] Department of Otorhinolaryngology, Jena University Hospital, Lessingstraße 2, 07743 Jena, Germany

[4] Jena Center for Soft Matter (JCSM), Friedrich Schiller University Jena, Philosophenweg 7, 07743 Jena, Germany

[5] Leibniz Institute of Photonic Technology, Albert-Einstein-Straße 9, 07745 Jena, Germany

Introduction

According to the World Health Organization, 14.1 million new cancer cases occurred in 2012 and 32.6 million people are living with cancer worldwide. In addition, different cancer types are among the leading causes of death worldwide. It is expected that the annual diagnosed cancer cases will rise to 22 million within the next two decades [1]. This development must be faced by strong research efforts aiming for an improved cancer diagnosis as well as a treatment with increased curing rates. Thereby, the enormous degree of heterogeneity within one cancer type or even within one tumor has to be taken into account [2–4].

Many analytical methods exist allowing for molecular diagnostics, e.g., polymerase chain reaction (PCR), real-time-PCR, fluorescence in situ hybridization (FISH), and expressional proteomics [5, 6]. Furthermore, mass spectrometric techniques, especially desorption electrospray ionization, are used for modern tissue and tumor analysis [7–10]. New research fields, e.g., multidisciplinary molecular pathologic epidemiology [4] or the combination of molecular profiling and multi-parametric in situ analysis [2], recognize the need to combine different analysis methods for an optimal outcome and understanding. In addition, modern imaging techniques, namely Raman spectroscopic and matrix-assisted laser

desorption/ionization (MALDI) mass spectrometric imaging (MSI), were successfully applied for (cancerous) tissue analysis. Nevertheless, up till now a lack of reliable tumor markers exist that can be used in clinical practice to tackle the problem of the inherent molecular heterogeneity of the disease and the uniqueness of each patient. As a consequence, there is a need for multidisciplinary research. Here, we describe a possible workflow by combining Raman spectroscopy and MALDI-MS as a potential tool to gain insights into the variable epithelial differentiation as an eventually first step of carcinogenesis.

Matrix-assisted laser desorption/ionization (MALDI) mass spectrometry imaging (MSI) has been demonstrated to be useful for multiple molecular profiling of solid tumors [11] enabling among others the classification of cancer subtypes by lipid MALDI-MS-profiles [12]. Recently, Krasny et al. demonstrated the high potential of MALDI-Fourier-transform ion cyclotron resonance (FT-ICR)-MSI to provide spatial segmentation maps for the lipid analysis of head and neck tumor tissue, which can reveal new insights into the metabolic organization of the carcinoma tissue [13]. Although MSI features a high molecular specificity, it is destructive and requires the application of a complex matrix, which is only specific for lipid or protein profiling. These drawbacks can be compensated by a combination with Raman imaging, which is a noninvasive optical spectroscopic approach and does not require any labels. Raman spectroscopy probes inherent molecular vibrations that provide a highly specific molecular fingerprint of the biochemical composition of, e.g., biological cells, tissues etc. [14]. An objective evaluation of the chemically specific Raman maps for a disease diagnosis, e.g., for cancer, requires a processing via mathematical approaches [15]. However, a direct molecular interpretation of tissue Raman spectra is still a great challenge. As a consequence, the strength of MALDI-MS imaging with its high molecular specificity can eventually help to interpret the Raman spectra.

In order to use both kinds of information together, a complex computational workflow or data pipeline has to be developed and demonstrated. Here, we report a workflow for combining MALDI-MSI with Raman-spectroscopic imaging in order to check the tissue prediction of one of these techniques. The general workflow for combining Raman spectroscopy and MALDI imaging was recently demonstrated by Fagerer et al. [16], Bocklitz et al. [17] and Ahlf et al. [18]. We applied a similar registration procedure as described in our previous work [17], but combine the approach with hematoxylin and eosin (H&E) staining, the gold standard of pathologic cancer diagnosis. This workflow allows the identification of certain tissue areas by a pathologist's annotation based on the H&E image followed by a Raman-spectroscopic and MALDI-M-spectrometric characterization. As a proof-of-principle, we demonstrate for a larynx carcinoma tissue section that the origin of Raman spectral signatures can be interpreted by using mass spectrometric information.

Materials and methods

Sample collection and preparation

A tissue sample from a patient with a larynx carcinoma was provided by the Department of Otorhinolaryngology of the Jena University Hospital. The local Ethics Committee granted the necessary approval under no. 3008-12/10. A 10 μm thick section of the human tissue sample was cut at –20 °C using a Leica CM1860 cryomicrotome (Leica Biosystems Nussloch GmbH, Germany) and placed on an indium tin oxide (ITO)-coated slide (Bruker Daltonik GmbH, Bremen, Germany). To prevent an alteration of the cryosection, the sample was dried on the slide and directly measured via Raman spectroscopy followed by MALDI imaging.

Raman imaging

For the Raman spectroscopic measurements a confocal Raman microscope (WITec GmbH, Ulm, Germany) equipped with a continuous wave diode-pumped solid-state laser operating at 514 nm (Cobolt) with a laser power of 15 mW before the microscope objective was used. The tissue sample was measured with a 50×/NA 0.8 objective (Zeiss, Jena,Germany). The back scattered light was spectrally separated with a 600 lines/mm grating and detected by using a charge-coupled device (CCD) camera with 1024×127 pixels, thermo-electric cooled down to –70 °C.

An area of 2×3 mm of the tissue sample was measured with the "Large Area" point-by-point scanning mode with a step size of 12.5 μm and 241 measured lines per image and 161 measured points per line. An acquisition time of 0.5 s per spectrum was applied. Thus, the total acquisition time took 21 h.

MALDI imaging

The MALDI analysis applying a matrix sensitive for lipids was directly started after the Raman-spectroscopic characterization of the tissue sample. Therefore, the ImagePrep device (Bruker Daltonik GmbH, Germany) was used to apply the matrix consisting of alpha-cyano 4-hydroxy cinnamic acid (5 mg/mL) in 50 % acetonitrile and 0.2 % trifluoroacetic acid onto the tissue sample following the standard protocol. MALDI-TOF analysis was performed on the UltrafleXtreme MALDI-TOF/TOF mass spectrometer (Bruker Daltonik GmbH, Germany) equipped with a 2000 Hz smartbeam laser detecting positive ions in the reflective mode. The FlashDetector combined with a minimum of 4 GHz digitizer allows for a mass resolving power up to 40,000 and 1 ppm mass accuracy. Spectra were acquired for the *m/z* range 200 to

1500. The MALDI imaging raster size was set to 25 μm and 200 laser shots were accumulated per raster spot. This value does not reflect the resolution of the MALDI scan, which depends on the applied matrix. If a higher resolution is needed, a matrix optimization has to be performed, e.g., utilizing a different matrix or changing the application to the matrix sublimation method. However, such a matrix optimization lies beyond the scope of our article. Here, the MALDI imaging step size was set twice as high as the Raman imaging step size. After averaging two adjacent Raman spectra, a spot size of similar to the MALDI-images was obtained. The acquisition time of the entire tissue slice was in the range of 20 h. For spectral acquisition, the FlexImaging 3.0 software (Bruker Daltonik GmbH, Germany) was used.

Hematoxylin and eosin staining

After the MALDI imaging, the tissue slice was stained with hematoxylin and eosin (H&E). For removing the matrix, the slide was washed two times with 100 % ethanol. Afterwards, the sample was stained according to a standard protocol. The slide was scanned using the Panoramic DESK (Sysmex Deutschland GmbH, Norderstedt, Germany) slide scanner and was histologically analyzed by an experienced histologist/pathologist.

Data analysis

All computations were done in the statistical language R [19]. The utilized packages where "SPATSTAT" [20], "readBrukerFlexData" [21], MASS [22], and "Peaks" [23]. The analysis started with importing both kinds of spectra (i.e., MALDI and Raman spectra) and the H&E image. Pretreatment of the Raman spectra included spatial averaging, background correction using the Sensitive Nonlinear-Iterative-Peak-Clipping (SNIP) algorithm, vector normalization, and a principal-component-analysis (PCA) for dimension reduction [24]. The MALDI spectra were vector normalized and a PCA dimension reduction was carried out. All Raman spectra and the H&E stained image were co-registered with the MALDI scan by means of a recently reported rigid registration procedure [17], so all images and scans could be handled with respect to the MALDI-coordinate system. As the annotation of an experienced pathologist was done on the H&E stained image, all areas could be described by four values: the RGB value of the H&E stain, the class label of the annotation, the MALDI spectrum, and the Raman spectrum. The spectral histopathology (SHP) [25, 26] was implemented using a linear-discriminant-analysis (LDA) [22].

Results and discussion

Co-registration and characterization

The combination of the two imaging methods Raman spectroscopy and MALDI spectrometry starts with the co-registration of all relevant images or scans [17]. For this purpose, we decided to use the MALDI coordinate system as reference and transformed the H&E stained image and the (preprocessed) Raman scan with respect to this reference grid. This transformation is visualized in Fig. 1. Here, Fig. 1A displays a MALDI score plot, where the first three scores are color coded in red, green, and blue. The corresponding image of the loadings can be found in the Supporting Information section (see Electronic Supplementary Material (ESM) Fig. S1). Next to this MALDI score plot the co-registered H&E image is depicted together with the annotations performed by an experienced pathologist (Fig. 1B). The pixelation of the H&E results from the co-registration onto the pixel size of the MALDI scan. The pathologist's annotation (Fig. 1B), however, was performed on the original high resolution H&E image (ESM Fig. S2) and yielded the following five groups: "benign squamous epithelium," "epithelial dysplasia," "muscle tissue," "grandular tissue," and "adipose tissue." In the following and throughout the article, the groups "benign squamous epithelium" and "epithelial dysplasia" are abbreviated by SE and ED, respectively. Based on the co-registration of the MALDI-scan, the Raman scan and the H&E stained image, mean MALDI-spectra and mean Raman spectra of the different tissue types (i.e., of the above mentioned pathologist's annotation) could be calculated (Fig. 1C and D). These mean spectra will be interpreted in the following.

For a detailed interpretation of the mean MALDI spectra, it is particularly interesting to analyze the mean spectrum of the ED annotated region (Fig. 1C). Therefore, we compared m/z peaks found within our mass spectra with values found in the literature about cancer tissue MALDI characterization. We were not aiming for identifying new m/z cancer markers. Several m/z peaks, which were recently identified as tumor markers, show an increased intensity compared with the mean MALDI spectrum assigned to SE area. The m/z 741.6 peak originating from the K+ adduct of sphingomyelin (SM) (34:1), which tends to promote tumorigenesis [27], was found to be overexpressed in thyroid [27, 28] and HER2-positive breast cancer samples compared with adjacent normal tissue [11]. The observed phosphatidylcholine (PC) 36:0 H+ adduct (m/z value 756.6) was characterized to be significantly higher in cancer regions of oral squamous cell carcinoma than in the stromal region [29]. Furthermore, the K+ adduct of phosphatidylcholine (PC) 36:0 (m/z value 772.6) was detected and proofed to be overexpressed in thyroid [28] and breast cancer [11]. Additionally, the m/z 798.6 peak, which can be assigned to the K+ adduct of PC 34:1 [11, 27, 28], was also found to be
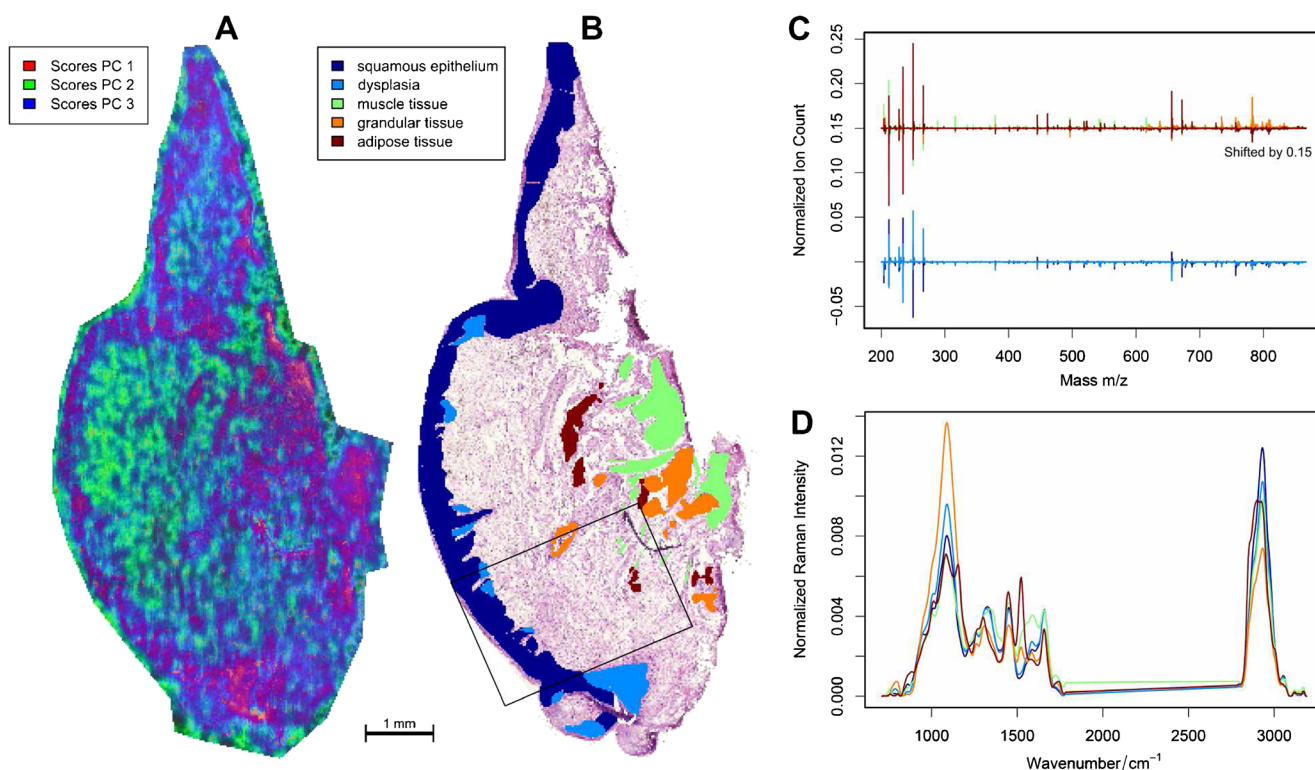
Fig. 1 (**A**) First three scores of a PCA from the MALDI data are visualized in false-colors (red/green/blue). See ESM Fig. S1 for the corresponding loadings plot. (**B**) H&E image with the overlaid annotation by a pathologist ("benign squamous epithelium," "epithelial dysplasia," "muscle tissue," "grandular tissue," and "adipose tissue") is given. The image shows pixelation attributable to the registration, while the original H&E stained image is given in ESM Fig. S2. The black rectangle indicates the Raman measured region. (**C**) Mean MALDI spectra of the pathologist's annotation (only Raman measured region) was plotted, where the mean MALDI spectrum of the whole data set was subtracted for clarity. (**D**) The mean Raman spectra of the pathologist's annotation are depicted. The scale bar represents 1 mm in (**A**) and (**B**), while the legend applies to panel (**B**), (**C**), and (**D**). See text for further details

overexpressed. In addition, the K+ adduct of PC 36:2 (*m/z* 824.6), which showed high intensities in cancer regions [11], is also present. Recently, Krasny et al. reported a high glycerophospholipids (GP) content inside head and neck tumor regions [13]. This is in accordance with our findings of several *m/z* values assigned to GPs inside the ED annotated region: **m/z** 772.6, 784.6, 796.6, 799.6, 804.7, 806.6, 808.7, 820.6.

The mean Raman spectra (Fig. 1D) are composed of two spectral regions, the fingerprint region from 700 to 1800 cm^{-1} and the CH–stretch region between 2800 and 3000 cm^{-1}, which shows the highest Raman peak intensities of the tissue spectra attributable to stretch vibration of the CH_2 and CH_3 groups present in all molecular tissue constituents like lipids, proteins, as well as nucleic acids [30]. The strong Raman signal at 1087 cm^{-1} present in all mean Raman spectra originates from the used ITO-coated cover slides. Thus, the prominent Raman peak of the symmetric ring breathing mode of phenylalanine at 1008 cm^{-1} is only visible as a small shoulder within the ITO Raman band. In contrast, the Raman peak of phenylalanine at 1588 cm^{-1} [31] is clearly visible and exhibits the highest intensity in the mean Raman spectra of the region annotated with muscle tissue. Further Raman peaks assigned to aromatic amino acids like tryptophan (754 cm^{-1} and

1554 cm^{-1}) and tyrosine 853 cm^{-1} occur in the mean Raman spectrum of muscle tissue since proteins are the main component of muscles [32]. In addition several Raman bands associated with collagen are visible at 1342 cm^{-1}, 1450 cm^{-1}, and as shoulders at 853 cm^{-1} and 1230 cm^{-1} in the mean Raman spectra of muscle tissue [31].

The mean Raman spectrum of the region annotated with adipose tissue is characterized by numerous prominent lipid Raman peaks, e.g., the shoulder at 3007 cm^{-1} [33], the peak at 2926 cm^{-1} [31, 33] and the shoulder at 2853 cm^{-1} [33, 34] can be assigned to unsaturated =CH, symmetric stretching vibration CH_2, and symmetric stretching vibration CH_3 originating from the acyl chains of fatty acids. Lipid Raman bands in the fingerprint region can be found at 1741 cm^{-1} (C=O stretch) [34], 1301 cm^{-1} (CH_2 twist) [31], and 1270 cm^{-1} (unsaturated fatty acid) [33]. The characteristic Raman peak at 1658 cm^{-1} has contributions of lipids (C=C stretch) as well as of the amide I vibration [30] typical for proteins. The mean Raman spectra of the regions annotated with SE and ED are very similar and display only small variations in intensity and wavenumber position of their Raman peaks, e.g., at 1658 cm^{-1} (amide I and lipids), 1588 cm^{-1} (phenylalanine), 1448 cm^{-1} (CH_2 deformation assigned to aliphatic amino

acids [31]) pointing towards structural changes mainly in the protein constitution during an ongoing dysplastic process.

Combining MALDI spectrometry and Raman spectroscopy

In order to check if the pathologist's annotation is reflected in the Raman spectra, we applied a spectral histopathology workflow recently reported by Diem et al. [25]. For this purpose, a PCA-LDA model was trained for the tissue-groups annotated by the pathologist within the Raman measured region. We introduced an additional "rest" group in order to account for regions that could not be annotated by the pathologist. The result of this training phase is displayed in Fig. 2A. A comparison of this training plot with the pathologist's annotation (Fig. 1B) shows a general agreement. In particular, the groups "muscle tissue," "glandular tissue," and "adipose tissue" coincide well. The main difference occurs in the prediction of SE and ED. Here, only the outer layer of the epithelium and the inner layer (basal layer) can be distinguished based on Raman spectroscopy. This may result from the fact

that the inner layer is the growing layer and the different metabolism is reflected in the Raman spectra.

This spectral histopathology Raman analysis reveals that Raman spectroscopy only allows for discriminating between the epithelial regions, which are proliferating, and other regions, which do not. The pathologist's annotation is more precise in this respect. As a consequence, we investigated the differences reflected within the MALDI spectra. For this purpose, we calculated the mean MALDI spectra of the following four regions: correctly Raman predicted as SE and ED, Raman predicted as SE but annotated by the pathologist as ED, and vice versa. The corresponding mean MALDI spectra of these four groups are highlighted in Fig. 2B, where the mean MALDI spectrum of the whole data set was subtracted for clarity.

Figure 2B shows that there are several m/z values exhibiting intensity differences for the four regions mentioned above. The intensities for the m/z 656 peak and the m/z 782 peak (H+ adduct of PC 36:4) [27] are lowest for the correctly Raman-predicted ED region and increase in the following order: region predicted as SE but annotated as ED, correctly predicted SE region, and region predicted as ED but annotated as SE. Therefore, the
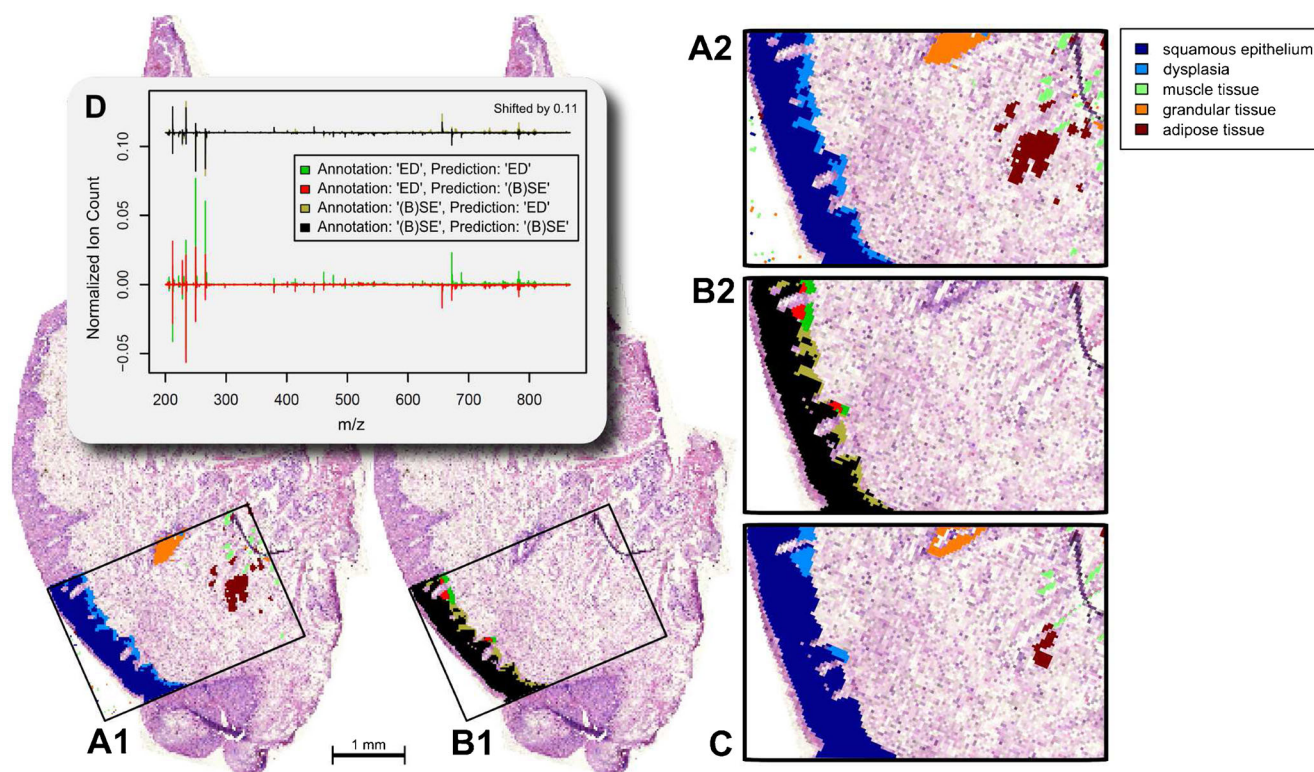

Fig. 2 (**A1/A2**) The PCA-LDA prediction of the Raman data is overlaid with H&E stain of the section, while the legend of Fig. 2 A2 applies. The Raman prediction unravels two layers, which may differ in their proliferation and thus metabolic status. These distinct layers can be interpreted as basal epithelial and differentiated epithelial layer. (**B1/B2**) The differences of the pathologist's annotation (Fig. 1B) and the Raman prediction (Fig. 2 A1/A2) are depicted for the groups "benign squamous epithelium" and "epithelial dysplasia." (**C**) The pathologist's annotation (Fig. 1B) was zoomed and displayed for comparison. (**D**) The

corresponding mean MALDI-spectra (with subtracted mean MALDI spectrum of the whole data set) for the four groups (false negative, true negative, false positive, and true positive) are depicted. It is clear that beside the Raman spectra not featuring strong differences, certain peaks in the mean MALDI spectra differ. These differences can be used to proof the origin of the Raman signatures. In the present case, normal epithelial growth can be distinguished from changed growth. The legend in (**C**) applies to (**B1/B2**) as well, whereas the legend of (**A2**) applies also to panel (**C**) and (**A1**). See text for details

intensity differences of these *m/z* values can help to distinguish between normal proliferating epithelial tissue and an ongoing dysplasia. The intensities for the *m/z* values at 461, 477, and 688 are similar for the region predicted as SE but annotated as ED, the correctly predicted SE region, and the region predicted as ED but annotated as SE, while they increase for the region correctly predicted as ED. Also for the *m/z* value 672 the highest intensity is observed for the region correctly predicted as ED and the intensity decreases in the following order: region predicted as ED but annotated as SE, correctly predicted SE region, and region predicted as SE but annotated as ED.

Conclusion

Here, we present a computational workflow for the combination of MALDI spectrometric imaging and Raman imaging. We demonstrated this combination workflow for a tissue sample from a patient with a larynx carcinoma. The combination started by co-registering the Raman scan and the H&E stained image to the MALDI grid as reference. Owing to this registration workflow the MALDI spectra and the Raman spectra could be analyzed together. In a first step, a spectral histopathology (SHP) analysis of the Raman spectra was carried out (Fig. 2). This SHP prediction was subsequently compared with the pathologist's annotation and diagnosis. The Raman based tissue classification yields a separation of the epithelial region into two layers differing in their metabolic state, which may be caused by a difference in proliferation and may coincide with the basal and differentiated epithelial layer.

In order to gain more insight, mean MALDI spectra of the dysplastic and benign epithelial regions were calculated dependent on if they were correctly Raman predicted or not. These four mean MALDI spectra of false-negative, true-negative, false-positive, and true-positive regions are given in Fig. 2C. The interpretation of these mean MALDI spectra can be used to unravel the prediction based on the Raman spectra. Therefore, the Raman spectra can be interpreted on a molecular level. Here, we applied a specific MALDI matrix for lipids, which allows us to understand which lipids are present in the four above-mentioned regions. Our present study shows that several *m/z* values, e.g., *m/z* 782 or *m/z* 672, correlate with the Raman based prediction as ED. With these *m/z* values, healthy growth in the basal layer can be distinguished from an altered growth leading to ED.

The methodology developed in this contribution enables a cross-check of either the SHP prediction based on MALDI spectrometry or the SHP prediction based on Raman spectroscopy with the other technique, respectively. Here, we demonstrate the cross-check of Raman spectroscopy based SHP. While Raman spectroscopic imaging can be utilized to determine the tissue type and the growth status of the epithelial layer, MALDI imaging probes the lipidome as we applied a matrix-specific for lipids. By this combination, one method (Raman spectroscopy) can be used to determine the tissue type and the other method (MALDI imaging) can be used to investigate changes occurring in this tissue type. In our present example, the combination allows for a better characterization of variable epithelial differentiation and yields a better understanding of ongoing dysplastic alterations. As an outlook, this computational workflow for combining different imaging methods may lead to a better understanding of the sample under investigation and may lead to markers for diseases or tissue types by combining the information from different analysis approaches. Such marker combinations applying different imaging methodologies may be the appropriate way to deal with the heterogeneity of tumors [2].

Conflict of interest The authors declare that no conflict of interest exists.

References

1. World Health Organization (2014) Global battle against cancer won't be won with treatment alone. Effective prevention measures urgently needed to prevent cancer crisis. On-line, Press Release No. 224

2. Almendro V, Marusyk A, Polyak K (2013) Cellular heterogeneity and molecular evolution in cancer. Annu Rev Pathol Mech 8:277–302

3. Cheng L, Alexander RE, MacLennan GT, Cummings OW, Lopez-Beltran A, Montironi R, Cramer HM, Davidson DD, Zhang S (2012) Molecular pathology of lung cancer: key to personalized medicine. Mod Pathol 25(3):347–369

4. Lochhead P, Chan AT, Giovannucci E, Fuchs CS, Wu K, Nishihara R, O'Brien M, Ogino S (2014) Progress and opportunities in molecular pathological epidemiology of colorectal premalignant lesions. Am J Gastroenterol 109(8):1205–1214

5. Netto GJ, Saad RD, Dysert PA (2003) Diagnostic molecular pathology: current techniques and clinical applications, part 1. Proc (Baylor Univ Med Cent) 16(4):379

6. Netto GJ, Saad R (2005) Diagnostic molecular pathology, part 2. Proteomics and clinical applications of molecular diagnostics in hematopathology. Proc (Baylor Univ Med Cent) 18(1):7

7. Eberlin LS, Norton I, Dill AL, Golby AJ, Ligon KL, Santagata S, Cooks RG, Agar NYR (2012) Classifying human brain tumors by lipid imaging with mass spectrometry. Cancer Res 72:645–654

8. Eberlin LS, Tibshirani RJ, Zhang L, Longacre TA, Berry GJ, Bingham DB, Norton JA, Zare RN, Poultsides GA (2014) Molecular assessment of surgical-resection margins of gastric

cancer by mass-spectrometric imaging. Proc Natl Acad Sci U S A 111:2436–2441

9. Takats Z, Wiseman JM, Gologan B, Cooks RG (2004) Mass spectrometry sampling under ambient conditions with desorption electrospray ionization. Science (Washington, DC) 306:471–473

10. Wiseman JM, Ifa DR, Song Q, Cooks RG (2006) Tissue imaging at atmospheric pressure using desorption electrospray ionization (desi) mass spectrometry. Angew Chem Int Ed 45:7188–7192

11. Kim IC, Lee JH, Bang G, Kim YH, Choi SH, Kim KP, Kim HK, Ro L (2013) Lipid profiles for HER2-positive breast cancer. Anticancer Res 33:2467–2472

12. Kang HS, Lee SC, Park YS, Jeon YE, Lee JH, Jung SY, Park IH, Jang SH, Park HM, Yoo CW, Park SH, Han SY, Kim KP, Kim YH, Ro J, Kim HK (2011) Protein and lipid MALDI profiles classify breast cancers according to the intrinsic subtype. BMC Cancer 11:465

13. Krasny L, Hoffmann F, Ernst G, Trede D, Alexandrov T, Havlicek V, Guntinas-Lichius O, von Eggeling F, Crecelius AC (2014) Spatial segmentation of MALDI FTICR MSI data: a powerful tool to explore the head and neck tumor in situ lipidome. J Am Soc Mass Spectrom 26:36–43

14. Schmitt PM, Popp J (2003) Raman spectroscopy—a prospective tool in the life sciences. Chem Phys Chem 4:14–30

15. Bocklitz T, Schmitt M, Popp J (2014) Ex-vivo and in-vivo optical molecular pathology, chapter 7. Image processing – chemometric approaches to analyze optical molecular images. Wiley-VCH Verlag GmbH & Co: KGaA, pp 215–248

16. Fagerer SR, Schmid T, Ibáñez AJ, Pabst M, Steinhoff R, Jefimovs K, Urban PL, Zenobi R (2013) Analysis of single algal cells by combining mass spectrometry with Raman and fluorescence mapping. Analyst 138(22):6732–6736

17. Bocklitz TW, Crecelius AC, Matthäus C, Tarcea T, Eggeling F, Schmitt M, Schubert US, Popp J (2013) Deeper understanding of biological tissue: quantitative correlation of MALDI-TOF and Raman imaging. Anal Chem 85(22):10829–10834

18. Ahlf DR, Masyuko RN, Hummon AB, Bohn PW (2014) Correlated mass spectrometry imaging and confocal Raman microscopy for studies of three-dimensional cell culture sections. Analyst 139: 4578–4585

19. R Development Core Team (2007) R: a language and environment for statistical computing. R Foundation for Statistical Computing, Vienna

20. Baddeley A, Turner R (2005) SPATSTAT: an R package for analyzing spatial point patterns. J Stat Softw 12(6):1–42

21. Gibb S (2013) readBrukerFlexData: reads mass spectrometry data in Bruker *flex format, R package version 1.7

22. Venables WN, Ripley BD (2002) Modern applied statistics with S, 4th edn. Springer, New York

23. Peaks MM (2008) Peaks R package version 0.2

24. Bocklitz T, Walter A, Hartmann K, Rösch P, Popp J (2011) How to pre-process Raman spectra for reliable and stable models? Anal Chim Acta 704:47–56

25. Diem D, Mazur A, Lenau K, Schubert J, Bird B, Miljković M, Krafft C, Popp J (2013) Molecular pathology via IR and Raman spectral imaging. J Biophoton 6(11/12):855–886

26. Bielecki C, Bocklitz TW, Schmitt J, Krafft C, Marquardt C, Gharbi A, Knösel T, Stallmach A, Popp J (2012) Classification of inflammatory bowel diseases by means of Raman spectroscopic imaging of epithelium cells. J Biomed Opt 17(7):076030

27. Guo S, Qiu L, Wang Y, Qin X, Liu H, He M, Zhang Y, Li Z, Chen X (2014) Tissue imaging and serum lipidomic profiling for screening potential biomarkers of thyroid tumors by matrix-assisted laser desorption/ionization Fourier transform ion cyclotron resonance mass spectrometry. Anal Bioanal Chem 406:4357–4370

28. Ryu J, Bang G, Lee JH, Choi SH, Jung YS, Kim KP, Kim YH, Kim HK (2013) Lipid MALDI MS profiling accurately distinguishes papillary thyroid carcinoma from normal tissue. J Proteom Bioinf 6:65–71

29. Uchiyama Y, Hayasaka T, Masaki N, Watanabe Y, Masumoto K, Nagata T, Katou F, Seto M (2014) Imaging mass spectrometry distinguished the cancer and stromal regions of oral squamous cell carcinoma by visualizing phosphatidylcholine (16:0/16:1) and phosphatidylcholine (18:1/20:4). Anal Bioanal Chem 406:1307–1316

30. Krafft C, Knetschke T, Siegner A, Funk RHW, Salzer S (2003) Mapping of single cells by near infrared Raman microspectroscopy. Vib Spectrosc 32(1):75–83

31. Krafft C, Codrich D, Pelizzo G, Sergo V (2009) Raman and FTIR imaging of lung tissue: bronchopulmonary sequestration. J Raman Spectrosc 40(6):595–603

32. Krafft C, Codrich D, Pelizzo G, Serg V (2008) Raman and FTIR microscopic imaging of colon tissue: a comparative study. J Biophotonics 1:154–169

33. Krafft C, Neudert L, Simat T, Salzer R (2005) Near infrared Raman spectra of human brain lipids. Spectrochim Acta A 61A:1529–1535

34. Krafft C, Knetschke T, Funk RHW, Salzer R (2005) Identification of organelles and vesicles in single cells by Raman microspectroscopic mapping. Vib Spectrosc 38:85–93
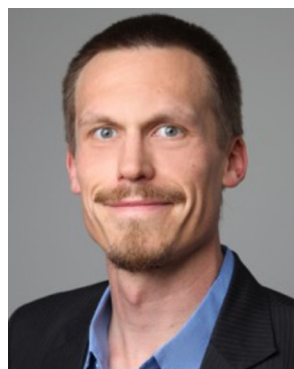
Thomas Bocklitz was born in 1982 and studied physics and mathematics at the Friedrich Schiller University. He received his diploma in theoretical physics in 2007 and the PhD in chemometrics in 2011. Dr. Thomas Bocklitz is a junior research group leader for statistical data analysis and image analysis, mostly for biophotonic applications. Dr. Bocklitz's research agenda is closely connected with the translation of physical information, measured by AFM, TERS, Raman-spectroscopy, CARS, SHG, TPEF, into medical or biological relevant information. This research led to 30 publications in peer-reviewed journals, one patent, and one book chapter.

Katharina Bräutigam successfully completed her first state examination in teacher study (biology and chemistry) and received her PhD in the research group of Professor Dr. Jürgen Popp at the Institute of Physical Chemistry and Abbe Center of Photonics at the Friedrich Schiller University Jena in 2015. Her research is mainly concerned with spectroscopic and spectrometric investigation of cancer cells and tissue.

Annett Urbanek was born 1979 in Jena. She finished her education as a medical lab technician in Jena in 2001. In 2002 she joined the Core Unit Chip Application of Professor F. von. Eggeling at the Jena University Hospital and was engaged with proteomic techniques and SELDI mass spectrometry until 2009. Since 2010 she is engaged in the field of applied MALDI mass spectrometry in the research group of Professor U.S. Schubert at the Friedrich Schiller University Jena.
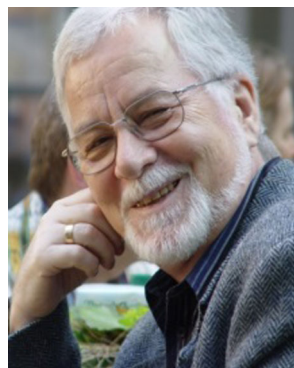
Günther Ernst studied medicine at the Friedrich Schiller University Jena, Germany, where he also received his MD in 1965 and completed the specialist training in pathology in 1972. In 1985 he became head of molecular diagnostics at the Institute of Human Genetics of the university hospital. Since 2011 he supports the Core Unit Chip Application (CUCA) at the same institute. Since 2013 he is affiliated with the ENT-Department of the University Hospital and the Leibniz Institute of Photonic Technology (IPHT) in Jena as pathologist.
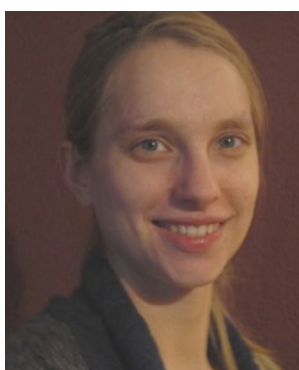
Franziska Hoffmann was born in 1988 and obtained her Diploma degree in biology at the Friedrich Schiller University Jena. Since 2014 she is working on her PhD thesis under the supervision of Professor F. von Eggeling. She is interested in molecular tumor fingerprints, and her research focuses on the characterization of head and neck tumor tissue using MALDI Imaging.

Michael Schmitt received his PhD in chemistry from the University of Würzburg in 1998. From 1999 to 2000 he went for postgraduate studies to the Steacie Institute for Molecular Sciences at the National Research Council of Canada. He subsequently joined the group of Professor Kiefer at the University of Würzburg, where he finished his habilitation in 2004. Since March 2004 he has been a research associate in the group of Professor Jürgen Popp at the Institute for Physical Chemistry at the Friedrich Schiller Universität Jena. His main research interests are focused on non-linear spectroscopy.

Ferdinand von Eggeling studied biology and chemistry in Erlangen and finished his PhD (1995) and his Habilitation (2003) at the Friedrich Schiller University Jena in Genetics. Since 2001 he was head of the Core Unit Chip Application (CUCA) at the Institute of Human Genetics. In 2009 he received the apl. Professor for Genetics at the Friedrich Schiller University Jena. Currently he has an affiliation at the Institute of Physical Chemistry and the ENT-Department of the University Hospital in Jena. His main interest is in mass spectrometric imaging of different tumor entities and the biological characterization of functional tissue components.

Ulrich S. Schubert studied chemistry in Frankfurt and Bayreuth and the Virginia Commonwealth University (USA). His PhD studies were performed at the Universities of Bayreuth and Tampa (USA). After postdoctoral training with Jean-Marie Lehn at the University of Strasbourg (France), he moved to the TU München and obtained his habilitation in 1999. From 1999 to 2000 he was Professor at the Center for NanoScience, University of Munich, and from 2000 to 2007 Full-Professor at TU Eindhoven (The Netherlands). Currently he holds a chair at the Friedrich Schiller University Jena with research interest in nanoparticle systems as sensor and drug delivery devices, supramolecular chemistry, inkjet printing of polymers, polymers for energy applications, and self-healing materials.

Orlando Guntinas-Lichius studied medicine at the University of Cologne, Germany. He completed specialist training in otorhinolaryngology at the Department of Otorhinolaryngology, University of Cologne in 1998 and worked in the department until 2006. In Cologne, he also finished his habilitation in 2001. Since 2006 he is Full Professor for Otorhinolaryngology and head of the Department of Otorhinolaryngology, Jena University Hospital, Jena, Germany. His main research interests are new diagnostics and treatment of head and neck cancer, treatment of salivary gland tumors, and improvement of functional regeneration after facial nerve reconstruction.

Jürgen Popp studied chemistry at the universities of Erlangen and Würzburg. After his PhD in Chemistry he joined Yale University for postdoctoral work. He subsequently returned to Würzburg University where he finished his habilitation in 2002. Since 2002 he holds a chair for Physical Chemistry at the Friedrich Schiller University Jena. Since 2006 he is also the scientific Director of the Leibniz Institute of Photonic Technology, Jena. His research interests are mainly concerned with biophotonics. In particular, his expertise in the development and application of innovative Raman techniques for biomedical diagnosis should be emphasized.